

Exploring Instance Relations for Unsupervised Feature Embedding

Yifei Zhang^{1,2}, Yu Zhou^{1*}, Weiping Wang¹

¹Institute of Information Engineering, Chinese Academy of Sciences

²School of Cyber Security, University of Chinese Academy of Sciences

{zhangyifei0115, zhouyu, wangweiping}@iie.ac.cn

Abstract

Despite the great progress achieved in unsupervised feature embedding, existing contrastive learning methods typically pursue view-invariant representations through attracting positive sample pairs and repelling negative sample pairs in the embedding space, while neglecting to systematically explore instance relations. In this paper, we explore instance relations including intra-instance multi-view relation and inter-instance interpolation relation for unsupervised feature embedding. Specifically, we embed intra-instance multi-view relation by aligning the distribution of the distance between an instance's different augmented samples and negative samples. We explore inter-instance interpolation relation by transferring the ratio of information from pixel space to feature embedding space. The proposed approach, referred to as EIR, is simple-yet-effective and can be easily inserted into existing view-invariant contrastive learning based methods. Experiments conducted on public benchmarks for image classification and retrieval report state-of-the-art or comparable performance. Our code will be available at <https://github.com/zhangyifei01/EIR>.

1 Introduction

Unsupervised feature embedding methods have attracted increased attention in recent years. As a mainstream method for unsupervised feature embedding, contrastive learning method focuses on learning an embedding function by attracting positive pairs and repelling negative pairs. However, it is challenging to discover positive and negative samples under unsupervised scenarios.

To discover reliable positive and negative samples on unlabeled datasets, instance discrimination based unsupervised methods have achieved promising results on unsupervised feature embedding. Instance Recognition (IR) [Wu *et al.*, 2018] proves that non-parametric instance-wise classification can capture apparent visual similarity. Invariant and Spreading Instance Feature (ISIF) [Ye *et al.*, 2019] exploits data

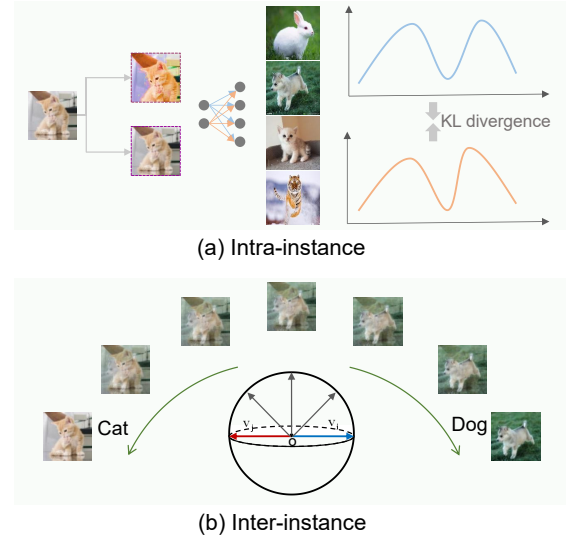


Figure 1: Illustrations of the instance relations including both intra-instance multi-view relation (a) and inter-instance interpolation relation in an unit sphere embedding space (b).

augmentation invariant and instance spreading property for unsupervised learning. Momentum Contrast (MoCo) [He *et al.*, 2020] build a dynamic dictionary with a queue and a moving-averaged encoder. After that, SimCLR [Chen *et al.*, 2020] simplifies these instance discrimination based contrastive learning algorithms without requiring specialized architectures. Compared with instance discrimination based unsupervised methods, supervised learning methods absorb more information from the different instances with same semantic categories. While instance discrimination based methods have shown their effectiveness on several benchmarks, they severely rely on single instance discrimination and data augmentation, and ignore the relations of instances, Figure 1. Augmentation Invariant and Spreading Instance Feature (aISIF) [Ye *et al.*, 2020] improves ISIF by two feature-level augmentation strategies including negative augmentation with interpolation and positive augmentation with extrapolation. However, the instance relations are still not systematically explored, which makes the learned feature embedding less discriminative.

*Corresponding author

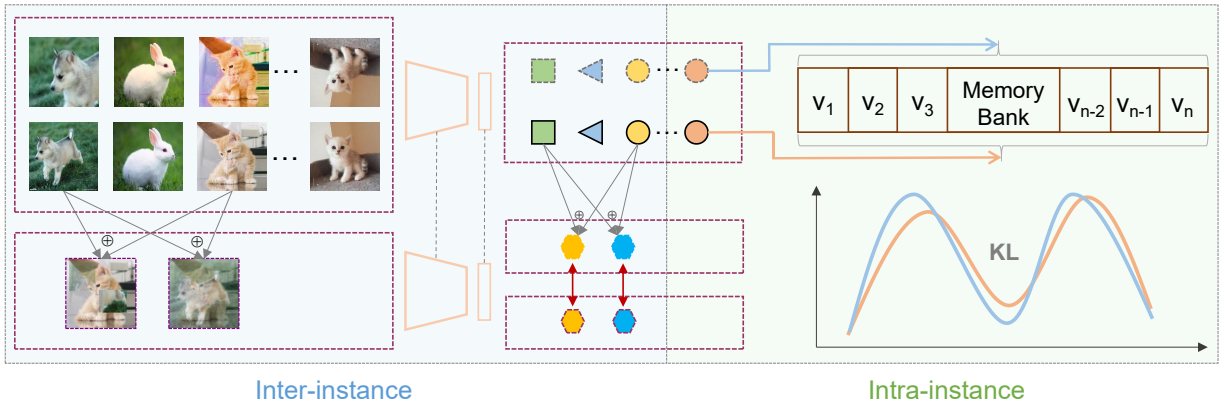


Figure 2: Overview of EIR, which includes intra-instance multi-view relation (left) and inter-instance interpolation relation (right). Different shapes represent different semantic categories, and different colors represent different instances.

In this paper, we present exploring instance relations (EIR) including both intra-instance multi-view relation and inter-instance interpolation relation for unsupervised feature embedding, Figure 2. Specifically, for exploring more sophisticated intra-instance relations, we align two distributions with KL divergence, each of which is the distance distribution of an augmented sample with respect to all samples in the training set, Figure 1(a). Benefiting from current data augmentation strategies such as mixup [Zhang *et al.*, 2018] and cutmix [Yun *et al.*, 2019], we explore inter-instance interpolation relation by transferring the ratio of information for image sample interpolation from pixel space to feature space, Figure 1(b). By simultaneously incorporating these two relations, our approach improves the capability of discrimination in the embedding space. Our approach is simple-yet-effective and can be easily inserted into existing view-invariant contrastive learning based methods.

We present extensive evaluations of our approach on various datasets and tasks to demonstrate its effectiveness. In particular, our method achieves the accuracy of 89.2% on CIFAR-10 in the kNN setting, which is the state-of-the-art performance to the best of our knowledge.

The contributions of this work are summarized as follows:

1. We propose EIR to systematically explore previous overlooked instance relations for unsupervised feature embedding, which is a novel attempt to break through the limit of instance discrimination.
2. We explore the intra-instance multi-view relation by aligning two augmented samples' distance distribution, which measures the relations of the augmented samples with respect to all samples in the training set.
3. We explore inter-instance interpolation relation by transferring the ratio of information for image sample interpolation from pixel space to feature space.
4. We conduct experiments for image classification and retrieval on CIFAR-10, STL-10, ImageNet-100, CUB-200 and Car-196 datasets. EIR achieves state-of-the-art or comparable performance.

2 Related Works

There are two related concepts in unsupervised deep learning methods: unsupervised representation learning and unsupervised embedding learning.

Unsupervised Representation Learning. Unsupervised representation learning aims at learning 'immediate' *conv* features, then the features can be used as the initialization for downstream tasks such as image classification and object detection. Some works focus on designing pretext tasks by hiding some information such as context prediction [Doersch *et al.*, 2015], jigsaw puzzle [Noroozi and Favaro, 2016], colorization [Larsson *et al.*, 2016], split-brain [Zhang *et al.*, 2017] and rotations prediction [Gidaris *et al.*, 2018].

Unsupervised contrastive learning based methods can be roughly categorized into two categories: instance-based methods and group-based methods. For instance-based methods, IR [Wu *et al.*, 2018] treats each sample as an independent class. Contrastive Multiview Coding(CMC) [Tian *et al.*, 2020] proposes to maximize the mutual information between different views and scales to any number of views. MoCo [He *et al.*, 2020] builds a dynamic dictionary with a queue and a moving-averaged encoder. After that, SimCLR [Chen *et al.*, 2020] simplifies these instance discrimination based contrastive learning algorithms without requiring specialized architectures or memory bank. For group-based methods, [Yang *et al.*, 2016] and DeepCluster (DC) [Caron *et al.*, 2018] joint clustering and feature learning by iteratively grouping features and using the assignments as pseudo labels to train feature representations. Anchor Neighbourhood Discovery (AND) [Huang *et al.*, 2019] adopts a divide-and-conquer method to find local neighbours. Local Aggregation [Zhuang *et al.*, 2019] trains an embedding function to maximize a metric of local aggregation. Online DeepCluster [Zhan *et al.*, 2020] performs clustering and network updating simultaneously rather than alternatively.

Unsupervised Embedding Learning. Unsupervised embedding learning focuses on learning a low-dimension feature embedding by minimizing the distance of positive pairs and maximizing the difference of negative pairs, and the learned *conv* features also can be used for initialization. Mining

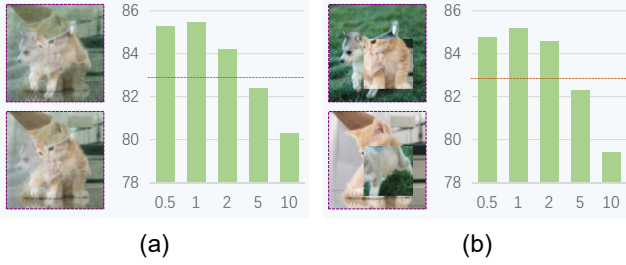


Figure 3: Illustrations of the instance interpolation operations and its performance under different coefficients. Dashed line denotes the accuracy for baseline method. (a) Mixup [Zhang *et al.*, 2018]; (b) Cutmix [Yun *et al.*, 2019].

on Manifolds [Isken *et al.*, 2018] proposes an unsupervised method to mine hard positive and negative samples based on manifold space. ISIF [Ye *et al.*, 2019] proposes to utilize the instance-wise supervision to approximate the positive concentration and negative separation properties, and aSIF [Ye *et al.*, 2020] improves ISIF by two feature-level augmentation strategies including negative augmentation with interpolation and positive augmentation with extrapolation. PSLR [Ye and Shen, 2020] incorporates adaptive softmax embedding in graph latent space. Current contrastive based unsupervised representation learning methods, *i.e.* IR [Wu *et al.*, 2018], MoCo [He *et al.*, 2020], can also be applied for unsupervised embedding learning.

3 Methodology

3.1 Preliminaries

Given an imagery data set $X = \{x_1, x_2, x_3, \dots, x_N\}$ without any manual annotations, the learned embedding model with parameters θ maps an input image x_i to a D -dimension embedding in feature space $\mathcal{V}(t)$ at t -th epoch, as $v_i(t) = f_{\theta_t}(x_i)$. The objective is to learn an embedding feature space where embedding for positive pairs are attracted while negative pairs are repelled. Details will be illustrated as follows.

IR [Wu *et al.*, 2018] proves that CNNs can capture apparent similarity and learn class discriminative feature representation with solely instance-level supervision. The probability of input x being recognized as i -th example is

$$P(i|v) = \frac{\exp(v_i^T v / \tau)}{\sum_{j=1}^N \exp(v_j^T v / \tau)}, \quad (1)$$

where $v = f_{\theta}(x)$, N is the size of whole dataset and τ is a temperature parameter. Objective function is defined as $L = -\sum_{i=1}^N \log P(i|f_{\theta}(x_i))$. IR maintains a memory bank for storing the global features of dataset, v_i and v_j in Eq.(1) denote the i -th and j -th features in memory bank. Memory bank is initialized as unit random vectors and evolves during training iteration by $v_i(t) = \ell_2((1-m) \times v_i(t) + m \times v_i(t-1))$.

Based on the analysis of IR, we modify instance recognition by applying multi-view data augmentation, which termed IRaug. The probability of an input x and its another view \hat{x}

being recognized as i -th example is

$$P(i|v, \hat{v}) = \frac{\exp(v_i^T v / \tau)}{\sum_{j=1}^N \exp(v_j^T v / \tau)} + \frac{\exp(v_i^T \hat{v} / \tau)}{\sum_{j=1}^N \exp(v_j^T \hat{v} / \tau)}. \quad (2)$$

IRaug forces v and \hat{v} to be close to the corresponding feature v_i in memory bank, is not just implementing IR twice. More specifically, it forces v and \hat{v} to be close to each other implicitly. We optimize the objective function by

$$L_{IRaug} = -\sum_{i=1}^N \log P(i|f_{\theta}(x_i), f_{\theta}(\hat{x}_i)). \quad (3)$$

We update memory bank with either of v or \hat{v} . IRaug will serve as our baseline in the following experiments.

3.2 Intra-instance Multi-view Relation

From the perspective of ISIF [Ye *et al.*, 2019] and MoCo [He *et al.*, 2020], view-invariant contrastive loss focuses on attracting different views of the same instance while repelling the different instances. However, more sophisticated intra-instance relations are not fully explored.

One such relation is that the current instance's two augmented samples should have similar distances with each sample in the training set. As illustrated in the right part of Figure 2. Concretely, other than only pushing negative samples far away, two augmented samples from the same instance should push the same negative sample to similar distances. Formally, for the two augmented samples from the same instance, two corresponding distance distributions can be obtained: D and \hat{D} ,

$$D = \{d_i = v^T v_i | i = 1, 2, 3, \dots, N\}, \quad (4)$$

and

$$\hat{D} = \{\hat{d}_i = \hat{v}^T v_i | i = 1, 2, 3, \dots, N\}. \quad (5)$$

These two distributions should be aligned. We define this relation as intra-instance multi-view relation, which can be modeled by the Kullback–Leibler divergence [Kullback, 1959] of distributions D and \hat{D} . By this way, the objective function is formed by

$$L_{intra} = \sum_{p=1}^N KL(D(p) || \hat{D}(p)), \quad (6)$$

where $D(p)$ denotes the distant distribution of current instance, and $\hat{D}(p)$ is that of another view.

3.3 Inter-instance Interpolation Relation

To address inter-instance relation, aSIF [Ye *et al.*, 2020] explores feature-level interpolation as negative samples by $v_{p-} = \ell_2(\alpha v_i + (1-\alpha)v_k)$, which consistently improves the performance. Inspired by this work, we move one more step to explore the inter-instance relation from pixel level to feature level.

Our hypothesis is that better features can be learned if the consistency of the pixel-level interpolation and the feature-level addition is maintained. As illustrated in the left part of Figure 2, if an image is composed of two images with

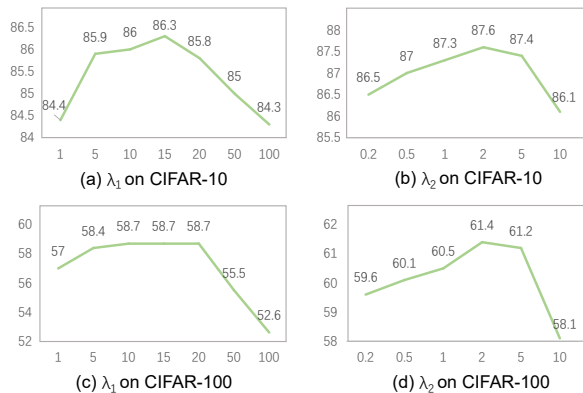


Figure 4: Effect of EIR with coefficient λ_1 and λ_2 on CIFAR-10 and CIFAR-100 datasets.

Table 1: Effect of the components in our approach with k NN top-1 accuracy on CIFAR-10, $k = 200$.

IRaug	Intra-instance	Inter-instance	Accuracy(%)
✓	-	-	83.4
✓	✓	-	86.3 (+2.9)
✓	-	✓	85.5 (+2.1)
✓	✓	✓	87.6 (+4.2)

some specific ratios by interpolation, its feature should be close to the addition of the two images’ features with corresponding ratios. Benefiting from current data augmentation strategies such as mixup [Zhang *et al.*, 2018] and cutmix [Yun *et al.*, 2019], inter-instance interpolation can be implemented by mixup or cutmix. More general, we explore interpolation by information fusion with different ratios, Figure 3 shows some possible interpolation alternatives and its performance.

For two random instances x_i and x_j in unlabelled dataset, we can extract partial information from x_i with ratio r and partial information from x_j with ratio $(1 - r)$ to form a new image sample. The feature embedding of interpolated sample is defined as

$$v^k = f_\theta(rx_i \oplus (1 - r)x_j), \quad (7)$$

where \oplus denotes interpolation operation, and r denotes the ratio of information for interpolation. Meanwhile, the feature addition in embedding space is generated by

$$\tilde{v}^k = \ell_2(rf_\theta(x_i) + (1 - r)f_\theta(x_j)), \quad (8)$$

where ℓ_2 denotes ℓ_2 normalization. By attracting these two features, the information ratio can be transferred from pixel space to feature space. The inter-instance interpolation relation loss is obtained by

$$L_{inter} = -\log \sum_{k=1}^N \frac{\exp((v^k)^T \tilde{v}^k / \tau)}{\sum_{j=1}^N \exp((v^j)^T \tilde{v}^k / \tau)}. \quad (9)$$

In summary, the overall loss function is a combination of the baseline loss L_{IRaug} , the intra-instance multi-view relation loss L_{intra} and the inter-instance interpolation relation loss L_{inter} , which is formulated as

$$Loss = L_{IRaug} + \lambda_1 L_{intra} + \lambda_2 L_{inter}. \quad (10)$$

Table 2: Comparison of k NN top-1 accuracy with different k on CIFAR-10 dataset. R denotes training round (200 epochs for 1 round). Performance of other methods is copied from PSLR [Ye and Shen, 2020] and aSIF [Ye *et al.*, 2020].

Methods	k=5	k=20	k=200
Random	32.4	34.8	33.4
IR	79.6	80.5	80.8
DC(1000)	66.5	67.4	67.6
ISIF	82.4	83.1	83.6
CMC	82.0	82.6	83.1
aSIF	86.4	87.0	86.6
PSLR	83.8	84.7	85.2
IRaug	81.5	83.4	83.4
Ours	86.6	87.5	87.6
AND(5Rs)	84.8	85.9	86.3
PSLR+(5Rs)	87.4	88.1	88.4
Ours(2Rs)	87.7	88.3	88.6
Ours(5Rs)	88.2	89.2	89.1

4 Experiments

We conduct extensive experiments to evaluate the proposed method on downstream tasks including classification and retrieval.

4.1 Experimental setting

Datasets. CIAFR-10/CIFAR-100 [Krizhevsky and Hinton, 2009] contains 50K training and 10K test images with 10/100 object classes, and all images are with size 32×32 . STL-10 [Coates *et al.*, 2011] contains 5K labeled images with 10 classes and 100K unlabeled images for training, and 8K images with 10 classes for testing, and all images are with size 96×96 . During pre-training, the labels are deleted. ImageNet [Russakovsky *et al.*, 2015] subset ImageNet-100 contains 126,689 images with 100 classes for training, and 5K images for testing, and all images are resized to 224×224 .

We split the 200 classes of CUB-200 [Wah *et al.*, 2011] into two parts. The first 100 classes with 5,864 images are used for training, and the last 100 classes with 5,924 images are used for testing, and all images are resized to 224×224 . We then split the 196 classes of Car-196 [Krause *et al.*, 2013] into two parts. The first 98 classes with 8,054 images are used for training, other 98 classes with 8,131 images are used for testing, and all images are resized to 224×224 .

Hyper-parameters. We adopt ResNet18 [He *et al.*, 2016] as the backbone, and initialize the learning rate as 0.03 with the decreasing strategy that the rate is scaled down by 0.1 at 120-th epoch and 0.01 at 160-th epoch. We set momentum to 0.9, weight decay to 0.0005, batch size to 128, temperature parameter τ to 0.1, and the embedding feature space dimension to 128. All experiments are implemented with 2 GeForce RTX 2080Ti GPUs.

Evaluation Metrics. We use a single center-cropped image for feature extraction in testing phase, and use linear classification and k NN to evaluate features on classification task.

Table 3: Evaluation on STL-10 dataset with ResNet-18 by performing linear classifier (LC) and k NN ($k=200$) top-1 accuracy. Performance of other methods is copied from PSLR [Ye and Shen, 2020] and aISIF [Ye *et al.*, 2020].

Methods	Pre-train	Fine-tune	LC	kNN
Random	-	5K	28.7	22.4
Supervised	5K	5K	83.0	82.9
IR	5K	5K	62.3	66.8
DC(100)	5K	5K	56.5	61.2
ISIF	5K	5K	69.5	74.1
aISIF	5K	5K	72.2	74.0
IRaug	5K	5K	69.6	70.0
Ours	5K	5K	76.4	78.2
AND	105K	5K	76.8	80.2
CMC	105K	5K	77.4	81.2
ISIF	105K	5K	77.9	81.6
PSLR	105K	5K	78.8	83.2
aISIF	105K	5K	82.8	83.9
IRaug	105k	5K	74.4	81.0
Ours	105K	5K	79.3	84.7

The retrieval performance is evaluated by the probability of correct matching in the top- k retrieval ranking list.

4.2 Ablation Study

We take IRAug as our baseline method, then analyze the effect of our proposed module. In Table 1, the baseline method achieves 83.4% top-1 k NN ($k=200$) accuracy on CIFAR-10 dataset with ResNet18. The experimental results show that compared with the baseline, intra-instance multi-view relation improves the accuracy by 2.9%, inter-instance interpolation relation improves the accuracy by 2.1%, moreover, combining these two components can improve the accuracy by 4.2%.

In Figure 4 (a) and (c), we analyze the effect of the coefficient λ_1 in our loss function by incorporating baseline and intra-instance multi-view relation loss on CIFAR-10 and CIFAR-100 dataset. The experimental results show that with proper λ_1 ($\lambda_1=15$) our model achieves 86.3% and 58.7% top-1 accuracy on CIFAR-10 and CIFAR-100, respectively. We then analyze the coefficient λ_2 of inter-instance interpolation loss. The effect of λ_2 is shown in Figure 4 (b) and (d) by fixing λ_1 in Eq. 10. With $\lambda_1=15$ and $\lambda_2=2$ in Eq. 10, EIR achieves the best top-1 k NN accuracy with 87.6% and 61.4% on CIFAR-10 and CIFAR-100, respectively.

4.3 Image Classification

After fully training networks, we then evaluate the quality of the learned visual representations and feature embedding on image classification. The backbone is ResNet18 and the classification is evaluated by k NN and linear classification. The k NN classification uses feature embedding directly. Linear classification (LC) needs to train a fully connected linear classifier which is initialized from scratch, and the convolution layers are frozen. Considering the difference of image

Table 4: Evaluation on ImageNet-100 dataset with ResNet-18 by performing linear classifier (LC) and k NN ($k=200$) top-1 accuracy.

Methods	LC	kNN
Random	6.0	11.0
IR	60.2	59.1
DC*	56.4	51.8
ISIF	62.5	59.5
MoCo	64.4	64.2
IRaug	61.5	61.5
Ours	66.4	66.5

Table 5: Comparison of retrieval performance on CIFAR-10, CIFAR-100, CUB-200 and Car-196. The performance of other methods is reimplemented with their released codes. We implement DC with contrastive loss under 1000 clusters, AND with 2 rounds under 1 neighbour.

Acc(%)	R@1	R@2	R@4	R@8	R@1	R@2	R@4	R@8
Dataset	CIFAR-10				CIFAR-100			
Random	25.0	40.1	58.2	75.8	8.2	13.1	19.8	29.4
IR	70.8	82.5	90.0	95.4	36.0	46.3	56.9	68.0
DC	75.2	83.5	89.2	93.4	36.3	46.3	56.9	66.8
ISIF	74.7	84.6	91.3	95.8	40.8	51.4	62.1	72.5
AND	77.4	85.8	92.2	96.3	41.8	52.0	62.8	72.8
IRaug	73.3	83.9	91.4	96.1	39.7	50.1	60.5	71.5
Ours	79.9	88.5	93.6	97.1	45.6	56.5	66.9	76.5
Dataset	CUB-200				Car-196			
Random	3.4	6.1	10.4	18.1	4.5	7.1	11.1	17.5
IR	8.0	12.7	20.1	30.3	19.9	27.6	37.4	49.4
DC*	7.9	12.7	20.5	30.8	15.7	22.1	31.6	43.4
ISIF	12.6	19.2	28.3	39.3	26.6	36.0	46.5	58.4
AND	11.9	18.8	26.8	38.7	22.6	30.8	41.3	53.7
IRaug	11.1	17.1	26.4	37.2	23.1	31.1	41.7	53.9
Ours	14.6	22.1	32.6	44.1	28.5	38.1	49.5	62.1

resolution for different datasets, we evaluate the performance on datasets from low resolution to high resolution.

As shown in Table 2, on CIFAR-10 dataset under 1-round training with k equal to 5/20/200, our proposed method consistently achieves the best performance. After 5-rounds training, our method achieves 89.2% for $k = 20$, which surpasses all other published methods. Moreover, the performance of our method with only 2-rounds training outperforms those of other methods with 5-rounds training. Because the performance of SimCLR [Chen *et al.*, 2020] relies on large batch size, MLP head and stronger data augmentation, it is infeasible to compare EIR with SimCLR under the similar experiment settings. The comparison of performance for different backbone is shown in the supplementary material.

We then conduct experiments on STL-10 dataset, and report LC results with *conv5* layer and k NN top-1 results with $k = 200$ on 5K labeled set under 5K and 105K pre-training

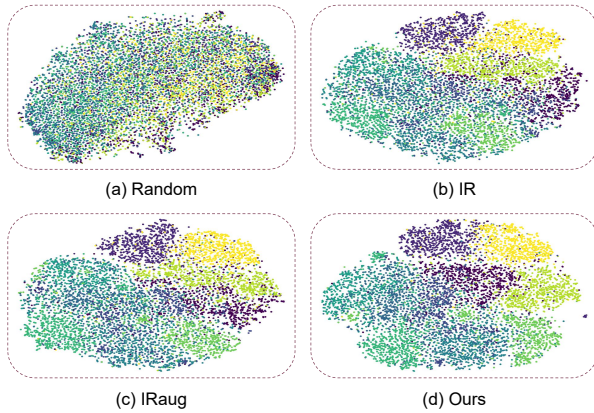


Figure 5: Visualization of embedding space by t-SNE. (Best viewed in color)

respectively. As shown in Table 3, our method achieves 76.4% accuracy with LC and 78.2% accuracy with kNN, which outperforms state-of-the-art aISIF [Ye *et al.*, 2020] by 4.2% on 5K pre-train setting. For 105K pre-train setting, our method achieves 84.7% accuracy with kNN, which outperforms aISIF by 0.8%. With LC, aISIF is superior to our method probably because our method needs more training iterations for convergence.

For ImageNet-100 evaluation, we report the LC results on *conv5* layer and kNN top-1 results with $k = 200$. As shown in Table 4, our method achieves 66.4% and 66.5% accuracy for LC and KNN respectively, which outperforms MoCo at least 2% accuracy and surpasses other methods with large margins.

4.4 Image Retrieval

Image retrieval experiments are conducted to evaluate the discriminative ability of the learned feature embedding. As shown in Table 5, EIR achieves 79.9%, 88.5%, 93.6% and 97.1% accuracy for R@1, R@2, R@4 and R@8 on CIFAR-10 dataset, and 45.6%, 56.5%, 66.9% and 76.5% accuracy on CIFAR-100 dataset, which shows the best performance on these two seen datasets.

For more challenging fine-grained unseen dataset, our method achieves 14.6%, 22.1%, 32.6% and 44.1% accuracy on CUB-200 dataset and 28.5%, 38.1%, 49.5% and 62.1% accuracy on Car-196 dataset, which achieves state-of-the-art performance. The retrieval performance on Car-196 surpasses the performance in CUB-200 with large margin, which may result from that birds are more hard to discriminate than cars.

4.5 Visualization

To show the effectiveness of positive pairs attracting while negative pairs repelling, we visualize the embedding features on test set of CIFAR-10 by embedding the feature embedding into 2-dimensional space with t-SNE [Van der Maaten and Hinton, 2008]. Figure 5 shows that instance discrimination based methods achieve the goal that positive attracting while negative pairs repelling, and our method is more discriminative.



Figure 6: The 8 nearest neighbourhood retrieval results by baseline method IRaug (top) and EIR (down). The positive retrieved results are framed in green while negative in pink.

To help qualitatively illustrate the effectiveness of our proposed method, Figure 6 shows the 8 nearest neighbourhood retrieval results on Car-196 test set including success and failure cases. The first column is 4 query images, and each one follows 2 rows retrieval results including IRaug (top) and EIR (down), and each row is ordered by cosine similarity. The 8 nearest neighbours of the 4-th query image are all false positive, they share high similarity on appearance, color and posture. However, from the results of first 3 query images, we can find that our model can discover positive samples with different colors, which shows that the features learned by our method focus on high-level semantic information.

5 Conclusion

In this paper, we present an unsupervised feature embedding method by exploring instance relations (EIR), which includes intra-instance multi-view relation and inter-instance interpolation relation. We explore intra-instance multi-view relation by aligning the distance distribution between two augmented samples and each sample in the training set. We then explore inter-instance interpolation relation by transferring the ratio of information for image sample interpolation from pixel space to feature space. Our experimental results show that our method achieves state-of-the-art or comparable performance on image classification and retrieval. In the future, more attention will be paid to relate the different instances of the same semantic category for unsupervised learning.

Acknowledgement

This work is supported by the National Key R&D Program of China (2017YFB1002400), the Open Research Project of the State Key Laboratory of Media Convergence and Communication, Communication University of China, China (No.

SKLMCC2020KF004), the Beijing Municipal Science & Technology Commission (Z191100007119002), the Key Research Program of Frontier Sciences, CAS, Grant NO ZDBS-LY-7024, the National Natural Science Foundation of China (No. 62006221).

References

- [Caron *et al.*, 2018] Mathilde Caron, Piotr Bojanowski, Armand Joulin, and Matthijs Douze. Deep clustering for unsupervised learning of visual features. In *ECCV*, pages 132–149, 2018.
- [Chen *et al.*, 2020] Ting Chen, Simon Kornblith, Mohammad Norouzi, and Geoffrey Hinton. A simple framework for contrastive learning of visual representations. In *ICML*, pages 1597–1607, 2020.
- [Coates *et al.*, 2011] Adam Coates, Andrew Ng, and Honglak Lee. An analysis of single-layer networks in unsupervised feature learning. In *AISTATS*, pages 215–223, 2011.
- [Doersch *et al.*, 2015] Carl Doersch, Abhinav Gupta, and Alexei A. Efros. Unsupervised visual representation learning by context prediction. In *ICCV*, pages 1422–1430, 2015.
- [Gidaris *et al.*, 2018] Spyros Gidaris, Praveer Singh, and Nikos Komodakis. Unsupervised representation learning by predicting image rotations. In *ICLR*, 2018.
- [He *et al.*, 2016] Kaiming He, Xiangyu Zhang, Shaoqing Ren, and Jian Sun. Deep residual learning for image recognition. In *CVPR*, pages 770–778, 2016.
- [He *et al.*, 2020] Kaiming He, Haoqi Fan, Yuxin Wu, Saining Xie, and Ross Girshick. Momentum contrast for unsupervised visual representation learning. In *CVPR*, pages 9729–9738, 2020.
- [Huang *et al.*, 2019] Jiabo Huang, Qi Dong, Shaogang Gong, and Xiatian Zhu. Unsupervised deep learning by neighbourhood discovery. In *ICML*, pages 2849–2858, 2019.
- [Iscen *et al.*, 2018] Ahmet Iscen, Giorgos Tolias, Yannis Avrithis, and Ondrej Chum. Mining on manifolds: Metric learning without labels. In *CVPR*, pages 7642–7651, 2018.
- [Krause *et al.*, 2013] Jonathan Krause, Michael Stark, Jia Deng, and Fei-Fei Li. 3d object representations for fine-grained categorization. In *ICCVW*, pages 554–561, 2013.
- [Krizhevsky and Hinton, 2009] Alex Krizhevsky and Geoffrey E. Hinton. Learning multiple layers of features from tiny images. In *Citeseer*, 2009.
- [Kullback, 1959] Solomon Kullback. *Information theory and statistics*. Wiley, 1959.
- [Larsson *et al.*, 2016] Gustav Larsson, Michael Maire, and Gregory Shakhnarovich. Learning representations for automatic colorization. In *ECCV*, pages 577–593, 2016.
- [Noroozi and Favaro, 2016] Mehdi Noroozi and Paolo Favaro. Unsupervised learning of visual representations by solving jigsaw puzzles. In *ECCV*, pages 69–84, 2016.
- [Russakovsky *et al.*, 2015] Olga Russakovsky, Jia Deng, Hao Su, Jonathan Krause, Sanjeev Satheesh, Sean Ma, Zhiheng Huang, Andrej Karpathy, Aditya Khosla, Michael Bernstein, Alexander C. Berg, and Fei-Fei Li. ImageNet large scale visual recognition challenge. *IJCV*, 115(3):211–252, 2015.
- [Tian *et al.*, 2020] Yonglong Tian, Dilip Krishnan, and Phillip Isola. Contrastive multiview coding. In *ECCV*, pages 776–794, 2020.
- [Van der Maaten and Hinton, 2008] Laurens Van der Maaten and Geoffrey Hinton. Visualizing data using t-sne. *JMLR*, 9(11):2579–2605, 2008.
- [Wah *et al.*, 2011] Catherine Wah, Steve Branson, Peter Welinder, Pietro Perona, and Serge Belongie. The caltech-ucsd birds-200-2011 dataset, 2011.
- [Wu *et al.*, 2018] Zhirong Wu, Yuanjun Xiong, Stella X. Yu, and Dahua Lin. Unsupervised feature learning via non-parametric instance discrimination. In *CVPR*, pages 3733–3742, 2018.
- [Yang *et al.*, 2016] Jianwei Yang, Devi Parikh, and Dhruv Batra. Joint unsupervised learning of deep representations and image clusters. In *CVPR*, pages 5147–5156, 2016.
- [Ye and Shen, 2020] Mang Ye and Jianbing Shen. Probabilistic structural latent representation for unsupervised embedding. In *CVPR*, pages 5457–5466, 2020.
- [Ye *et al.*, 2019] Mang Ye, Xu Zhang, Pong C. Yuen, and Shih-Fu Chang. Unsupervised embedding learning via invariant and spreading instance feature. In *CVPR*, pages 6210–6219, 2019.
- [Ye *et al.*, 2020] Mang Ye, Jianbing Shen, Xu Zhang, Pong C Yuen, and Shih-Fu Chang. Augmentation invariant and instance spreading feature for softmax embedding. *TPAMI*, 2020.
- [Yun *et al.*, 2019] Sangdoon Yun, Dongyoon Han, Sanghyuk Chun, Seong Joon Oh, Youngjoon Yoo, and Junsuk Choe. Cutmix: Regularization strategy to train strong classifiers with localizable features. In *ICCV*, pages 6022–6031, 2019.
- [Zhan *et al.*, 2020] Xiaohang Zhan, Jiahao Xie, Ziwei Liu, Yew Soon Ong, and Chen Change Loy. Online deep clustering for unsupervised representation learning. In *CVPR*, pages 6688–6697, 2020.
- [Zhang *et al.*, 2017] Richard Zhang, Phillip Isola, and Alexei A. Efros. Split-brain autoencoders: Unsupervised learning by cross-channel prediction. In *CVPR*, pages 1058–1067, 2017.
- [Zhang *et al.*, 2018] Hongyi Zhang, Moustapha Cissé, Yann N. Dauphin, and David Lopez-Paz. mixup: Beyond empirical risk minimization. In *ICLR*, 2018.
- [Zhuang *et al.*, 2019] Chengxu Zhuang, Alex Lin Zhai, and Daniel Yamins. Local aggregation for unsupervised learning of visual embeddings. In *ICCV*, pages 6002–6012, 2019.